Computation of electron-impact total and differential cross sections for allene (C_3H_4) in the energy range 0.1–2000 eV

Avani Barot,[1] Dhanoj Gupta,[2] Minaxi Vinodkumar,[1] and Bobby Antony[2,*]
[1]*V P & R P T P Science College, Vallabh Vidyanagar 388 120, Gujarat, India*
[2]*Department of Applied Physics, Indian School of Mines, Dhanbad 826004, Jharkhand, India*
(Received 4 April 2013; revised manuscript received 8 May 2013; published 3 June 2013)

In the present article we report a comprehensive calculation of total and differential cross sections for electron impact on allene (C_3H_4) molecule. The total cross sections are computed for a wide electron energy range from 0.1 eV to 2 keV. We have employed *R*-matrix code through QUANTEMOL-N software for *ab initio* calculations below 10 eV while intermediate- to high-energy calculations are performed using the spherical complex optical potential formalism. The two methods are found to be consistent at around 3 eV, merging smoothly. The results for both total and differential cross sections are in good agreement with previous results wherever available. We have also observed the presence of a shape resonance at 2.9 eV due to degenerate ($^2B_1$, $^2B_2$) states. The electronic excitation cross section for e-C_3H_4 scattering is reported.

DOI: 10.1103/PhysRevA.87.062701 PACS number(s): 34.80.Bm, 34.80.Ht

I. INTRODUCTION

The study of electron-impact total cross sections for hydrocarbons plays an important role in varieties of applications such as radiation biochemistry, low-temperature processing plasmas, atmospheric and astrophysical phenomena, and modeling electron assisted processes in fuel combustion [1–3]. Since the early 1930s, there has been interest in studying the relationship between the structural properties of the target and the shape and magnitude of the total cross sections (TCS) [4–6]. Recently the study of electron-impact total cross sections with C_3H_4 has geared up as it is the simplest hydrocarbon with isomeric effect. C_3H_4 molecule has two stable isomeric molecular structures, viz., allene and propyne. Allene has one carbon atom with a double bond with each of its two adjacent carbon centers. The reactivity of allene with gaseous chlorine is more like that of alkynes than alkenes and hence is much more reactive than other alkenes [7]. The central carbon of allene forms two sigma bonds and two pi bonds (Fig. 1) with hydrogen atom. The central carbon is sp hybridized, and the two terminal carbons are sp^2 hybridized, with a linear geometry for the carbons of allene. Owing to the simple structure and stability, C_3H_4 is a good candidate for investigation for both theoreticians as well as experimentalists. Besides, C_3H_4 is a feed gas in plasma enhanced chemical vapor deposition for the growth of carbon nanotubes [8]. Hence, it is imperative to study the electron-impact scattering on allene to understand various processes in these environments.

There are many studies concentrating on the isomeric effect of C_3H_4, its properties, and cross sections resulting from interaction with electrons. Nakano *et al.* [9] measured the absolute differential cross section (DCS) for C_3H_4 isomers (allene and propyne) from 1.5 to 100 eV. Szmytkowski and Kwitnewski [10] and Makochekanwa *et al.* [11] measured electron-impact TCS for C_3H_4 isomers at low energies from 0.5 to 370 eV and from 0.8 to 600 eV, respectively. Lopes and Bettega [12] and Sanchez *et al.* [13] calculated elastic and differential cross sections at low energies using Schwinger multichannel method. From the literature survey it is very clear that there are more experimental investigations [9–11] as compared to theory [12,13]. It is also noteworthy to see that there are no theoretical or experimental results beyond 600 eV. Thus, the studies on e-C_3H_4 scattering are fragmentary. Also, there is no comparison for electronic excitation cross sections in the literature to the best of our knowledge. Thus, in this article we present a comprehensive study that includes eigenphase diagram, electronic excitation cross sections, differential cross sections, and total and ionization cross sections over an extensive range of impact energies starting from very low energy of 0.1 to 2000 eV. Apart from the differential and total cross sections, we have also calculated total inelastic cross section comprised of total ionization and sum total of electronic excitations cross sections. Total ionization cross sections are then derived from Q_{inel} using the complex spherical potential-ionization contribution (CSP-ic) method [14]. These Q_{ion} are compared with the values reported by Kim and Irikura [15] using the binary-encounter-Bethe (BEB) method along with present computed BEB data through QUANTEMOL-N.

The central idea behind the present study is to investigate all the phenomena that occur in an electron-impact scattering over a wide energy range from 0.1 to 2000 eV. At low electron-impact energies (<10 eV) short-lived anions (resonances) may be formed which may then subsequently decay to produce neutral and anionic fragments. Hence, the prediction of low-energy resonance formation, which is strongly linked with the forces acting on the electrons during the scattering process and therefore the structural properties of the target, can be of utmost importance in understanding the local chemistry. However, intermediate- to high-energy electron scattering cross sections are required in other fields such as astrophysics, atmospheric physics, and radiation physics, where high-energy radiations such as x rays, cosmic rays, etc., are present and interact with gases. These high-energy interactions can produce an avalanche of secondary electrons which then provide the low-energy electrons for further chemical reactions. Consequently,

*bka.ism@gmail.com

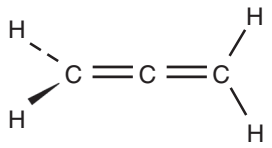

FIG. 1. Structure of allene.

there is a need for electron-impact scattering cross sections over a wide energy range from meV to keV.

In the next section we will present a detailed theoretical methodology adopted to evaluate various cross sections reported here.

II. THEORETICAL METHODOLOGY

The present calculations are performed using two distinct formalisms in two prime regimes of energy. The low-energy *ab initio* calculation (<10 eV) is carried out using UK molecular *R*-matrix code through QUANTEMOL-N [16] software package. For the intermediate to high energy, the well-established spherical complex optical potential (SCOP) [17–20] is used from 3 eV to 2 keV. Before going into the details of the theoretical methodologies, it is necessary to discuss the target model used for the low-energy calculation, since a correct representation of target wave function ensures accurate and reliable results.

A. Target model

Allene (C_3H_4) has trigonal planar geometry, connected at the ends by linear carbon atoms and in the middle with two double bonds (C=C). We have used 6-31G* Gaussian basis set for our target wave function representation. C_3H_4 has a D_{2d} point group symmetry; however, in our calculation we have used the C_{2V} point group, due to the limitation of QUANTEMOL-N software. The Hartree-Fock electronic configuration of the ground state is $1a_1^2$, $2a_1^2$, $3a_1^2$, $4a_1^2$, $5a_1^2$, $6a_1^2$, $7a_1^2$, $1b_1^2$, $1b_2^2$, $2b_2^2$, $2b_1^2$. Out of the total 22 electrons, we have frozen six core electrons in $1a_1$, $2a_1$, and $3a_1$ molecular orbitals, while the remaining 16 electrons are kept free in the active space of 11 molecular orbitals ($4a_1$, $5a_1$, $6a_1$, $7a_1$, $8a_1$, $1b_1$, $2b_1$, $3b_1$, $1b_2$, $2b_2$, $3b_2$). A total of 33 target states are represented by 2377 configuration state functions for the ground state, and the number of channels included in the calculation is 207.

Employing the present target model yields a ground state energy of −115.89 hartrees, which is in very good agreement with the value of −115.82 hartrees reported by Peyerimhoff and Buenker [21]. The present computed dipole moment in the equilibrium geometry comes out to be zero, agreeing with Lopes and Bettega [12]. On the other hand, the experimentally reported dipole moment is 0.2 a.u. by Nakano *et al.* [9]. The rotational constant obtained in the present calculation is 4.8066 cm^{-1} which is in excellent agreement with the CCCBDB database [22]. The calculated excitation energy from ground state to $^1A_2$ state is 6.60 eV which is in good agreement with the values of Rauk *et al.* [23], Diamond and Segal [24], Galasso and Fronzoni [25], and Jackson *et al.* [26] as evident from Table I.

B. Low-energy formalism (0.1 eV to ∼10 eV)

The Kohn variational method [27,28], Schwinger variational method [29–31], and the *R*-matrix method [18] are the three most popular methodologies used for low-energy calculations, of which the *R*-matrix method is the most widely used approach. The *R*-matrix method relies on the division of configuration space into two spatial regions, namely, an inner region and an outer region. The inner region is a sphere of radius '*a*' about the center of mass of the target called the *R*-matrix radius. The inner region has a radius of around 10 a.u. while the outer region is infinite. The calculations are done within a fixed-nuclei approximation which neglects any dynamics involving the nuclear motion (rotational and vibrational), whereas the bound electrons are considered in the electronic ground state of the target at its optimized nuclear geometry. This is an effect of the extent of electronic charge density distribution around the center of mass of the target. The choice of inner region is done so that it accommodates the total wave function of the target molecule. In the inner region, we cannot distinguish between the scattering electron and the electrons of the target, which makes the problem numerically complex but precise. The quantum chemistry codes are employed to solve the bound state problem of the inner region. The interaction potential consists of short-range

TABLE I. Target properties.

	Ground state energy (hartrees)		Dipole moment (a.u.)			First excitation energy E_1 (eV)		Rotational constant (B) (cm^{-1})		
Target	Present	Theor.	Present	Theor.	Expt.	Present	Theor.	Present	Theor.	Expt.
C_3H_4	–115.89	–115.82[a]	0.0	0[b]	0.2[c]	6.60	6.49[d] 6.56[f] 6.86[g] 6.23[h]	4.80	4.89[e]	4.81[e]

[a]Reference [21].
[b]Reference [12].
[c]Reference [9].
[d]Reference [23].
[e]Reference [22].
[f]Reference [24].
[g]Reference [25].
[h]Reference [26].

potentials which are dominant in the inner region. They are static, exchange, and correlation-polarization potentials. Moreover, the inner region problem is solved independent of the energy of the scattering electron and hence done only once. However, when the scattering electron is far away from the target electron cloud (i.e., in the outer region), there is no residual molecular charge density and hence the exchange and correlation effects are assumed to be negligible. Here only the long-range multipolar interaction between the scattering electron and the target are included. A single center approximation is assumed here which makes the problem simple, allowing it to converge quickly. For the present e-C_3H_4 system the inner R-matrix radius is taken as $10a_o$ while the outer region calculations are carried out up to $100\,a_o$ and found to give consistent results.

We construct the wave function for the inner region using the close coupling (CC) approximation [32] which is used to solve the time-independent Schrödinger equation and is given by

$$\psi_k^{N+1} = A\sum_I \psi_I^N(x_1,\ldots,x_N)\sum_j \zeta_j(x_{N+1})a_{Ijk} + \sum_m \chi_m(x_1,\ldots,x_{N+1})b_{mk}, \quad (1)$$

where A is the antisymmetrization operator, obtained by imposing Pauli's exclusion principle on the electrons. ψ_I^N is the wave function of target, x_N is the spatial and spin coordinate of the nth target electron, ξ_j is a continuum orbital spin-coupled with the scattering electron, and a_{Ijk} and b_{mk} are variational coefficients determined by the diagonalization of the Hamiltonian matrix. The first summation runs over the target plus continuum states used in the close-coupled expansion. The second term is called the L^2 term and the summation runs over configurations χ_m, where all electrons are placed in orbitals associated with the target. These χ_m are multicenter quadratically integrable functions constructed as the target wave functions, from the target occupied and virtual molecular orbitals. They are used to represent short-range correlations and polarization effects. The number of these configurations varies considerably with the model employed. Thus it can provide a good description of the electron correlations in several excited states of the molecule. With the wave function given by Eq. (1), a static exchange calculation has a single Hartree-Fock target state in the first sum. The second sum runs over the minimal number of configurations, usually three or fewer, required to relax orthogonality constraints between the continuum orbitals and those belonging to the target, given that the continuum orbitals are forced to be orthogonal to the target ones. Our fully close-coupled calculation uses the lowest number of target states, represented by a configuration interaction expansion in the first expansion and over a thousand configurations in the second. For the present problem we have used the eight lowest energetically excited target states. These configurations allow for both orthogonality relaxation and short-range polarization effects.

The complete molecular orbital representation in terms of occupied and virtual target molecular orbitals are constructed using the Hartree-Fock self-consistent field method using Gaussian-type orbitals and the continuum orbitals of Faure *et al.* [33] and included up to g ($l = 4$). In the case of dipole-forbidden excitations ($\Delta J \neq 1$) (where J is the rotational constant without spin coupling) the convergence of the partial waves is rapid. However, in the case of dipole-allowed excitations ($\Delta J = \pm 1$) the partial wave expansion converges slowly due to the long-range nature of the dipole interaction. The R matrix provides a link between the inner region and the outer region. For this purpose the inner region is propagated to the outer region potential until its solutions match with the asymptotic functions given by the Gailitis expansion [34]. The coupled single center equations describing the scattering in the outer region are integrated to identify the K-matrix elements. The K matrix is a symmetric matrix whose dimensions are the number of open channels. All the observables can be deduced from the K matrix and is used to obtain T matrices using the definition

$$T = \frac{2iK}{1 - iK}. \quad (2)$$

The T matrices are in turn used to obtain the physically observable quantities such as cross sections. The K matrix is diagonalized to obtain the eigenphase sum, which is further used to obtain the position and the width of the resonances by fitting the curve with Breit-Wigner form [35]. Further, the calculation of differential cross section involves the processing of K matrices through the method given by Sanna and Gianturco [36].

C. High-energy formalism (3 eV to 2 keV)

The electron-molecule scattering interactions can lead to different processes which can be broadly classified into elastic and inelastic processes. The total cross section is the sum of both, given as

$$Q_T(E_i) = Q_{el}(E_i) + Q_{\text{inel}}(E_i). \quad (3)$$

In SCOP formalism the Schrödinger equation is solved numerically to obtain complex phase shifts for each partial wave using the Numerov method. These phase shifts contain the signature of the scattering between the projectile and the target. At low impact energies only a few partial waves are significant, but as the electron energy increases, more and more partial waves are required for convergence. The phase shifts obtained are then used to calculate the appropriate cross sections [37] through

$$Q_{el}(E_i) = \frac{\pi}{k^2}\sum_{l=0}^{\infty}(2l+1)|\eta_l \exp(2i\,\text{Re}\delta_l) - 1|^2, \quad (4)$$

and

$$Q_{\text{inel}}(E_i) = \frac{\pi}{k^2}\sum_{l=0}^{\infty}(2l+1)\left(1-\eta_l^2\right). \quad (5)$$

Here k is the wave vector. The "inelasticity" or "absorption" factor for each partial wave 'l' is given by

$$\eta_l = \exp(-2\text{Im}\delta_l). \quad (6)$$

From Q_{inel}, the total ionization cross section, Q_{ion}, can be estimated using the CSP-ic method [14]. A detailed description of the CSP-ic method is given in Ref. [14] and references

therein. Here we have assumed a single center approach for the target, where the charge density of each atom is expanded from the center of mass of the system. The parametrized Roothaan-Hartree-Fock wave functions given by Cox and Bonham [38] are employed to find the charge density of atoms. The expansion will depend on the geometry of the target and mass of atoms in the molecule. The total charge density is then renormalized to account for the total number of electrons in the system. The final potential is assumed to be spherical and complex which depends upon the radial distance 'r' and incident energy E_i; hence the name spherical complex optical potential method. The final optical potential is given by

$$V_{\text{opt}}(r, E_i) = V_R(r) + i\,V_I(r, E_i). \tag{7}$$

Here the first term represents the real potential of the electron-target system and second term gives the absorption potential. The real potential of the present electron-target interaction is obtained by employing different model potentials, given as

$$V_R(r, E_i) = V_{st}(r) + V_{ex}(r, E_i) + V_p(r, E_i). \tag{8}$$

For the static potential (V_{st}) we have used the Cox and Bonham parameters [38], the exchange potential (V_{ex}) is obtained from the parameter-free Hara's [39] free electron gas exchange model, and for the polarization potential (V_p), the correlation potential of Zhang *et al.* [40] is used. The imaginary part of Eq. (7) takes care of the loss of the flux into various inelastic channels and is given by the model potential of Staszewska *et al.* [41] as

$$V_{abs}(r, E_i) = -\rho(r)\sqrt{\frac{T_{\text{loc}}}{2}}\left(\frac{8\pi}{10k_F^3 E_i}\right)\theta\left(p^2 - k_F^2 - 2\Delta\right) \times (A_1 + A_2 + A_3), \tag{9}$$

where the local kinetic energy of the electron is given by

$$T_{\text{loc}} = E_i - (V_{st} + V_{ex} + V_p). \tag{10}$$

Here, $p^2 = 2E_i$ and $k_F = [3\pi^2\rho(r)]^{1/3}$ is the Fermi wave vector. The functions A_1, A_2, and A_3 depend on the Heaviside unit step function $\theta(x)$, ionization threshold (I), energy parameter (Δ), and E_i. Δ is the factor that limits the effect of inelastic processes. In the original model of Staszewska *et al.* [41] the parameter Δ is fixed at the ionization potential. This assumption is not true as electronic excitations starts below the ionization threshold as their threshold usually falls below ionization potential. Hence, this has been modified by us by assuming Δ as a gradually varying function of energy near the ionization potential of the target. The approximation is meaningful as Δ fixed at I would not allow low-energy excitations and high-energy inner shell ionizations.

After obtaining the full complex optical potential for a given electron-molecule system, the Schrödinger equation is solved using the method of partial waves.

III. RESULTS AND DISCUSSION

In the present work, a detailed study of the electron scattering with allene (C_3H_4) molecule is performed. We have made use of two distinct formalisms for the calculation of total cross section for allene in the energy range from 0.1 eV to 2 keV. The low-energy calculations from 0.1 to 10 eV is carried out using UK molecular R-matrix code through QUANTEMOL-N. For intermediate to high energy (3 eV to 2 keV) SCOP formalism is employed. In the present study we have also calculated the elastic differential cross section and electronic excitation cross section from 1 to 15 eV and total ionization cross section from ionization threshold to 2 keV. The R-matrix calculations for the present target are done; hence it is of great significance to locate the resonance structure, if any, by studying the eigenphase diagram. The results so obtained are consistent and show a smooth transition at the overlap of the two formalisms for the TCS data. Hence, it is possible for us to predict the cross section for such a wide energy range. The results obtained are tabulated in Table II and are presented in graphical form in Figs. 2–6.

Figure 2 shows the eigenphase diagram for various doublet scattering states ($^2A_1$, $^2A_2$, $^2B_1$, and $^2B_2$) of the C_3H_4 system. In the low-energy regime, the study of the eigenphase sum finds significance as it reflects the position of resonance structure which is an important feature in this energy range and can lead to anion formation. The position and width of resonance

TABLE II. Total cross sections (TCS) for e-C_3H_4 scattering in Å^2.

Energy (eV)	TCS	Energy (eV)	TCS	Energy (eV)	TCS	Energy (eV)	TCS
0.1	18.33	4	37.23	20	36.48	160	15.95
0.2	19.80	5	33.84	26	35.20	180	14.79
0.3	20.17	6	32.90	30	34.20	200	13.84
0.5	20.04	7	33.37	36	32.68	250	11.97
0.7	19.73	8	34.02	40	31.69	300	10.57
1.0	19.44	9	34.68	46	30.28	400	8.64
1.3	19.34	10	35.27	50	29.36	500	7.33
1.5	19.36	11	35.67	60	27.28	600	6.39
1.8	19.65	12	36.08	70	25.43	700	5.66
2.0	20.22	13	36.37	80	23.79	800	5.09
2.4	24.48	14	36.60	90	22.32	900	4.63
2.8	41.73	15	36.73	100	21.07	1000	4.25
3.0	49.30	16	36.82	120	18.99	1500	3.02
3.5	38.75	18	36.77	140	17.32	2000	2.34

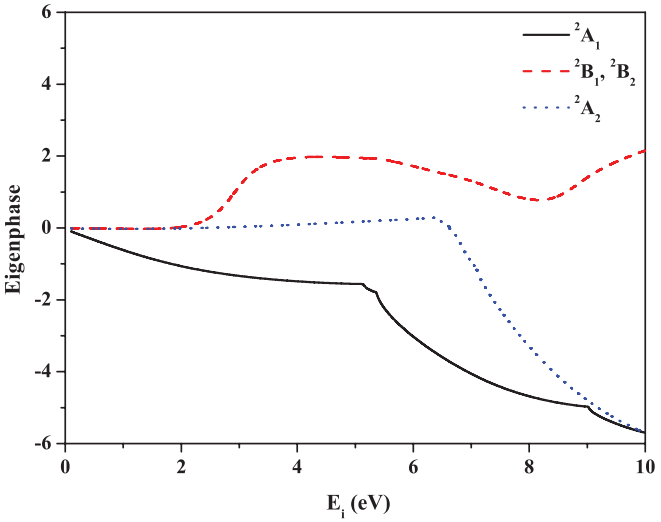

FIG. 2. (Color online) C_3H_4 eigenphase sums for a 33-state CC calculation.

states are listed in Table III with available comparison. $^2B_1$ and $^2B_2$ are the degenerate doublet states and are shown as a single curve in the eigenphase diagram. The $^2B_1$ and $^2B_2$ states show a prominent structure around 3 eV which confirms the presence of shape resonance in this energy range and is also reflected as a sharp peak in the TCS curve. As the ionization potential of allene is 9.69 eV, the R-matrix calculation is done up to 10 eV and SCOP is employed from 3 eV where elastic cross sections are computed by SCOP and excitation cross sections are obtained from R-matrix calculations. It is quite clear that below the ionization threshold of the target the TCS is the sum of total elastic cross section plus excitation cross sections. We have obtained a broad peak which is in good agreement with the experiments of Szmytkowski and Kwitnewski [10] and Makochekanwa *et al.* [11] from 10 to 20 eV in terms of the nature and shape of the cross section. The proper inclusion of electron correlations for the target and scattering wave function are very important in order to get the correct positioning of the resonances and the low-energy behavior of the cross section.

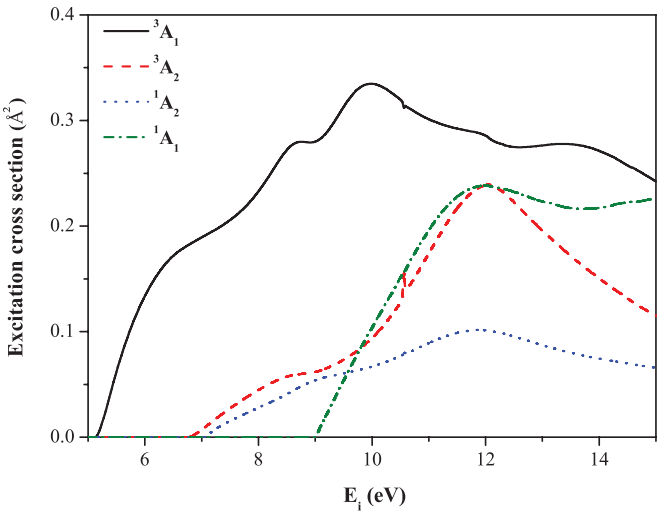

FIG. 3. (Color online) Excitation cross section for a 33-state CC calculation from the ground state.

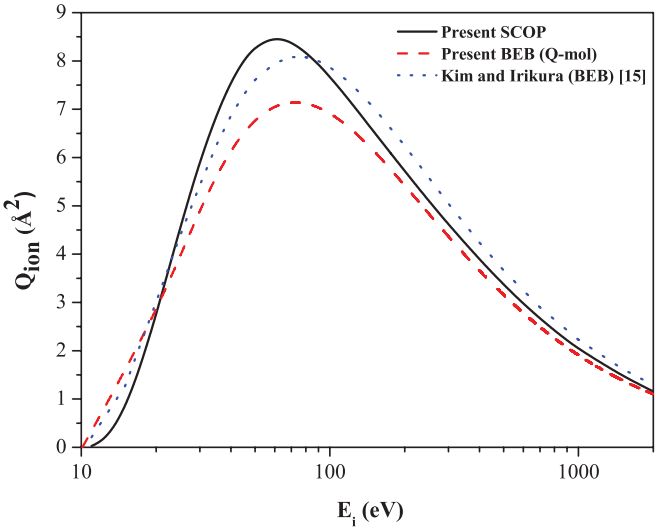

FIG. 4. (Color online) Q_{ion} for e-C_3H_4 scattering in Å^2. Solid line: present CSP-ic; dashed line: present BEB (Q-mol); dotted line: Kim and Irikura [15].

The cross sections for electronic excitation from ground state to the excited states $^3A_1$, $^3A_2$, $^1A_2$, and $^1A_1$ are given in Fig. 3. The electronic excitations to $^3A_1$ and $^1A_1$ show a sharp rise near their thresholds due to the dominance of these energy levels in the present calculation. The notable structure in $^3A_1$ around 10 eV is reflected as a hump around 10 eV in TCS.

The Q_{ion} derived using CSP-ic method for allene by electron impact is plotted in Fig. 4. Here we have compared our results with the theoretical BEB data obtained through QUANTEMOL-N and BEB data reported by Kim and Irikura [15]. Except at lower energies the present theory compares well

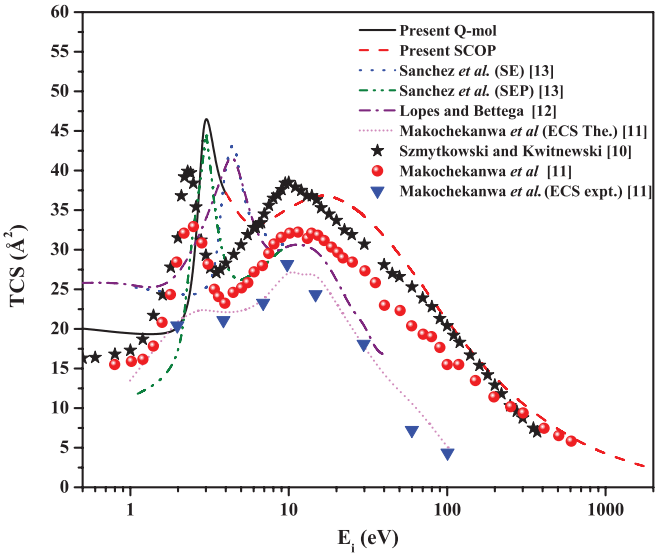

FIG. 5. (Color online) Total cross section (TCS) for e-C_3H_4 scattering system in Å^2. Solid line: present Q-mol; dashed line: present SCOP; dotted line: Sanchez *et al.* (SE) [13]; dash-dot-dot line: Sanchez *et al.* (SEP) [13]; dash-dot-dash line: Lopes and Bettega [12]; short dot line: Makochekanwa *et al.* (ECS) [11]; stars: Szmytkowski and Kwitnewski [10]; circles: Makochekanwa *et al.* [11]; inverted triangle: Makochekanwa *et al.* (ECS expt.) [11].

with BEB theory. However, the BEB cross section obtained in our calculation is slightly lower than other values reported here.

In Fig. 5 we have compared the present calculated TCS data for e-C_3H_4 over a wide range of energy from 0.1 eV to 2 keV with the available experimental and theoretical data. The present result shows a good matching at the overlap of the two formalisms and hence helps us to predict the cross section for such a wide energy range. In general a qualitative agreement is found between our calculated TCS in terms of position of the peak, maximum value of the cross section and the shape of the TCS curve with the available theoretical

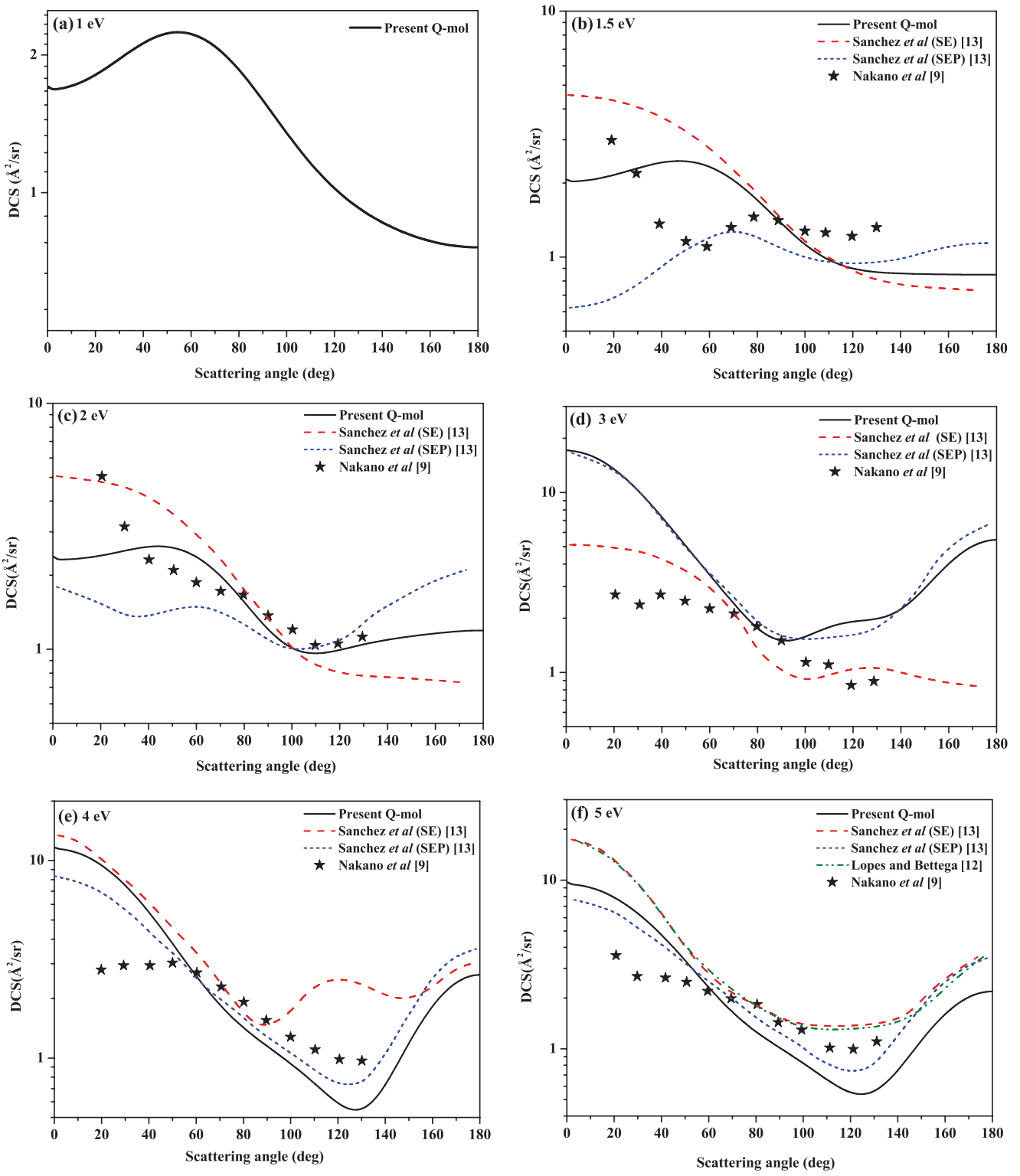

FIG. 6. (Color online) (*Continued.*)

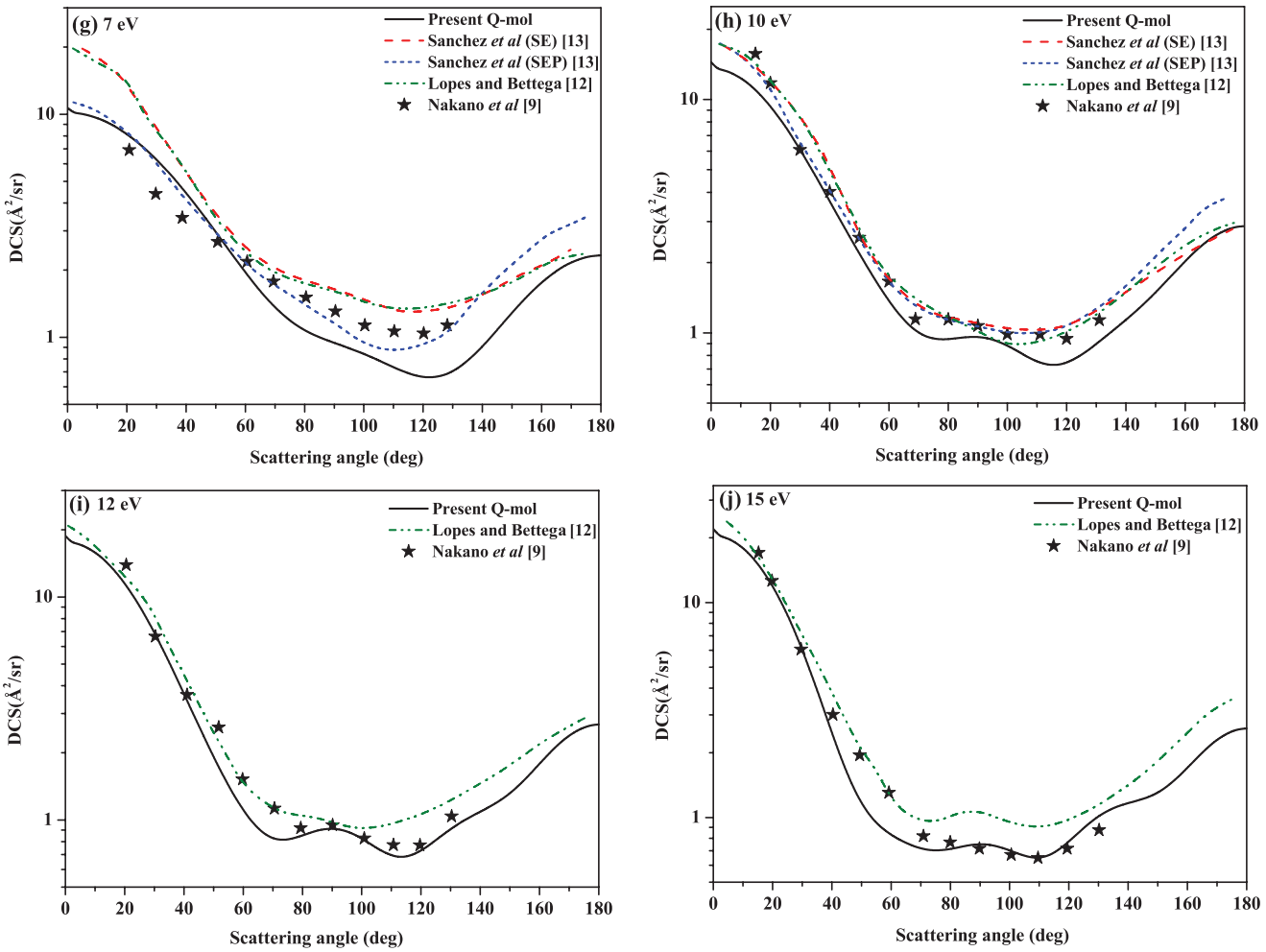

FIG. 6. (Color online) Differential cross section for e-C_3H_4 scattering system in Å^2 from 1 to 15 eV. Solid line: present Q-mol; dashed line: Sanchez *et al.* (SE) [13]; dotted line: Sanchez *et al.* (SEP) [13]; Dash-dot-dot line: Lopes and Bettega [12]; stars: Nakano *et al.* [9].

data [12,13]. Also a good comparison is found in terms of shape and nature of the curve with the experimental data of Szmytkowski and Kwitnewski [10]. The cross section of this molecule presents a shape resonance belonging to the twofold-degenerate E symmetry of the D_{2d} group, which splits into the $^2B_1$ and $^2B_2$ symmetries of the C_{2V} group. The present resonance peak matches very well with the static exchange plus polarization (SEP) result of Sanchez *et al.* [13] who have done the calculation using the Schwinger multichannel method. The peak value reported by the static exchange (SE) calculation of Sanchez *et al.* [13] and that of Lopes and Bettega [12] is shifted towards the higher-energy region since they have not included polarization in their calculation. The shape resonance reported by Szmytkowski and Kwitnewski [10] is at 2.3 eV with a peak value of 39.9 Å^2 which is quite close to the present peak located at 2.9 eV with a peak value of 45.98 Å^2. It is worth noting that the present calculations do not include the vibrational channel. The inclusion of the vibrational channel will reduce the peak of the cross section curve at low energy and will also increase the width of the curve, hence the small disagreement with experiments [10,11]. The elastic cross section of Makochekanwa *et al.* [11] also shows a shape resonance at 2.5 eV with the magnitude of cross section a little lower than all other results plotted in the graph, including the present one as they represent elastic cross sections.

In Figs. 6(a)–6(j) we have plotted the differential cross section for elastic scattering of allene at respective energies 1, 1.5, 2, 3, 4, 5, 7, 10, 12, and 15 eV at scattering angles 0°–180°. The calculated DCS are compared with the crossed-beam experimental results of Nakano *et al.* [9] and the theoretical Schwinger multichannel results of Sanchez *et al.* [13] and Lopes and Bettega [12]. After 5 eV the present DCS shows a good agreement with the experimental results of Nakano *et al.* [9] for all other energies. Except for 1.5 and 2 eV, the present DCS also shows decent agreement with the static exchange plus polarization (SEP) calculation of Sanchez *et al.* [13] for all other energies computed by them. The static exchange (SE) calculation of Sanchez *et al.* [13] and Lopes and Bettega [12] shows discrepancies at low incident energies that may be due to the exclusion of polarization effects. The DCS curve at 3 eV shows a hump at a scattering angle of around 120° which confirms the shape resonance at 2.9 eV in the TCS curve. The DCS at 10–15 eV also shows a humplike structure at a scattering angle around 90° which can be seen as the broad peak at those energies in the TCS curve.

TABLE III. Comparison of resonance position and width obtained in the present calculation with previous studies.

	Present		Others
Symmetry	Resonance position (eV)	Resonance width (eV)	Resonance position (eV)
$^1\Sigma^+(^2A_1)$	11.39; 12.37	3.75; 0.09	(9.5–10)[a] 11.0[b]
$^2\Pi$ ($^2B_1$, $^2B_2$)	2.90	0.86	2.3; 0.8[a] 2.5[b]
$^2\Sigma^-$ ($^2A_2$)	14.02	0.64	–

[a]Reference [10].
[b]Reference [11].

IV. CONCLUSIONS

In the present work a detailed study of the e-C_3H_4 system is done in terms of eigenphase diagram, total and differential cross sections, excitation cross section, and total ionization cross section. The total cross section is reported over a wide range of impact energies from 0.1 eV to 2 keV using two distinct formalisms. We have employed the UK molecular R-matrix code using QUANTEMOL-N at low impact energies and SCOP formalism at intermediate and high energies. The presence of shape resonance at 2.9 eV due to degenerate ($^2B_1$, $^2B_2$) states of the C_{2V} symmetry is reflected as a strong peak of 49.3 Å at around 3 eV. Moreover, the eigenphase diagram and the differential cross section at 3 eV also show a humplike structure which further confirms the resonance at that energy. There are only two calculations done for this molecule at low-energy regime using the Schwinger multichannel method. The present calculation at low energies matches very well with Sanchez *et al.* [13] including the positioning of their peak as well as the magnitude of the total cross section. At the transition point the cross section matches fairly well and helps us in predicting the cross section for such a wide energy range. At high energies our TCS shows very good agreement with the experimental results of Szmytkowski and Kwitnewski [10]. We have also reported the electron excitation cross section. The total ionization cross section reported here compares well with the existing data of the BEB model [15].

The total cross section data presented here find a variety of applications from aeronomy to plasma modeling, atmospheric sciences, etc. Accordingly, such a methodology may be built into the design of an online database to provide "data users" with the opportunity to request their own set of cross sections for use in their own research. Such a prospect will be explored by the emerging Virtual Atomic and Molecular Data Centre (VAMDC) [42].

ACKNOWLEDGMENTS

M.V. and B.A. are thankful to Department of Science and Technology, New Delhi, for financial support through Project Grants No. SR/S2/LOP-26/2008 and No. SR/FTP/PS-27/2009, respectively, under which part of this work was carried out.

[1] N. Kaifu, in *Molecular Processes in Space*, edited by T. Watanabe, I. Shimamura, M. Shimizu, and Y. Itikawa (Plenum, New York, 1990), pp. 205–231.
[2] W. L. Morgan, Adv. At. Mol. Opt. Phys. **43**, 79 (2000).
[3] K. Tanaka and M. Inokuti, Adv. At. Mol. Opt. Phys. **43**, 1 (2000).
[4] E. Brüche, Ann. Phys. Lpz. **388**, 1065 (1927).
[5] E. Brüche, Ann. Phys. Lpz. **396**, 387 (1930).
[6] F. Schmieder, Z. Elektrochem. Angew. Phys. Chem. **36**, 700 (1930).
[7] R. B. Daniel, *Organic Chemistry Demystified* (McGraw-Hill, New York, 2012).
[8] J.-H. Han, T. Y. Lee, J.-B. Yoo, C.-Y. Park, T. Jung, J. M. Kim, S. G. Yu, and W. Yi, J. Vac. Sci. Technol. B **21**, 1720 (2003).
[9] Y. Nakano, M. Hoshino, M. Kitajima, H. Tanaka, and M. Kimura, Phys. Rev. A **66**, 032714 (2002).
[10] C. Szmytkowski and S. Kwitnewski, J. Phys. B **35**, 3781 (2002).
[11] C. Makochekanwa, H. Kawate, O. Sueoka, M. Kimura, M. Kitajima, M. Hoshino, and H. Tanaka, Chem. Phys. Lett. **368**, 82 (2003).
[12] A. R. Lopes and M. H. F. Bettega, Phys. Rev. A **67**, 032711 (2003).
[13] S. d'A. Sanchez, A. R. Lopes, M. H. F. Bettega, M. A. P. Lima, and L. G. Ferreira, Phys. Rev. A **71**, 062702 (2005).
[14] R. Naghma and B. Antony, Mol. Phys. **111**, 269 (2013).
[15] Y.-K. Kim and K. K. Irikura, in *Proceedings of 2nd International Conference on Atom. Molec. Data and Their Application*, edited by K. A. Berrington and K. L. Bell (AIP, New York, 2000) [AIP Conf. Proc. **543**, 220 (2000)].
[16] J. Tennyson, Phys. Rep. **491**, 29 (2010).
[17] M. Vinodkumar, A. Barot, and B. Antony, J. Chem. Phys. **136**, 184308 (2012).
[18] M. Vinodkumar, H. Bhutadia, B. K. Antony, and N. J. Mason, Phys. Rev. A **84**, 052701 (2011).
[19] R. Naghma, B. N. Mahato, M. Vinodkumar, and B. K. Antony, J. Phys. B **44**, 105204 (2011).
[20] D. Gupta and B. Antony, J. Electron Spectrosc. Relat. Phenom. **186**, 25 (2013).
[21] S. D. Peyerimhoff and R. J. Buenker, Theor. Chim. Acta (Berl.) **14**, 305 (1969).
[22] See http://cccbdb.nist.gov/.
[23] A. Rauk, A. F. Drake, and S. F. Mason, J. Am. Chem. Soc. **101**, 2284 (1979).

[24] J. Diamond and G. A. Segal, J. Am. Chem. Soc. **106**, 952 (1984).
[25] V. Galasso and G. Fronzoni, J. Mol. Struct. **133**, 235 (1985).
[26] W. M. Jackson, A. M. Mebel, S. H. Lin, and Y. T. Lee, J. Phys. Chem. A **101**, 6638 (1997).
[27] B. I. Schneider and T. N. Rescigno, Phys. Rev. A **37**, 3749 (1988).
[28] T. N. Resigno, C. W. McCurdy, A. E. Orel, and B. H. Lengsfield III, in *Computational Methods for Electron Molecule Collisions*, edited by W. M. Huo and F. Gianturco (Plenum Press, New York 1995), pp. 1–44.
[29] K. Takatsuka and V. McKoy, Phys. Rev. A **24**, 2473 (1981).
[30] K. Takatsuka and V. McKoy, Phys. Rev. A **30**, 1734 (1984).
[31] C. Winstead, Q. Y. Sun, P. G. Hipes, M. A. P. Lima, and V. Mckoy, Aust. J. Phys. **45**, 325 (1992).
[32] A. M. Arthurs and A. Dalgarno, Proc. Phys. Soc. London, Sect. A **256**, 540 (1960).
[33] A. Faure, J. D. Gorfinkiel, L. A. Morgan, and J. Tennyson, Comput. Phys. Commun. **144**, 224 (2002).
[34] M. Gailitis, J. Phys. B **9**, 843 (1976).
[35] G. Breit and E. Wigner, Phys. Rev. **49**, 519 (1936).
[36] N. Sanna and F. A. Gianturco, Comput. Phys. Commun. **114**, 142 (1998).
[37] C. J. Joachain, *Quantum Collision Theory* (North-Holland, Amsterdam, 1983).
[38] H. L. Cox and R. A. Bonham, J. Chem. Phys. **47**, 2599 (1967).
[39] S. Hara, J. Phys. Soc. Jpn. **22**, 710 (1967).
[40] X. Zhang, J. Sun, and Y. Liu, J. Phys. B **25**, 1893 (1992).
[41] G. Staszewska, D. W. Schwenke, D. Thirumalai, and D. G. Truhlar, Phys. Rev. A **28**, 2740 (1983).
[42] M. L. Dubernet, V. Boudon, J. L. Culhane, M. S. Dimitrijevic, A. Z. Fazliev, C. Joblin, F. Kupka, G. Leto, P. Le Sidaner, P. A. Loboda, H. E. Mason, N. J. Mason, C. Mendoza, G. Mulas, T. J. Millar, L. A. Nuñez, V. I. Perevalov, N. Piskunov, Y. Ralchenko, G. Rixon *et al.*, J. Quant. Spectrosc. Radiat. Transfer **111**, 2151 (2010).